Research Article | DOI:10.5281/zenodo.18063940
www.jnanosam.com

NANOSAM
Journal of NanoScience in Advanced Materials

Towards a Pressure-Sensitive FET-Based Sensor for Urodynamic Pressure Mapping

Ahmed Harb[1#] and Mustafa İstanbullu[2]

Bladder dysfunctions, including urinary incontinence and neurogenic bladder, affect millions of individuals worldwide and are most commonly diagnosed using invasive, catheter-based urodynamic studies. While clinically reliable, these methods are uncomfortable, infection-prone, and unsuitable for long-term monitoring. This study presents the design and simulation of a MEMS-based pressure sensor utilizing a molybdenum disulfide (MoS_2) field-effect transistor (FET) architecture for continuous bladder monitoring. The device operates through a suspended diaphragm that deflects under applied pressure, modulating the effective gate capacitance and thereby altering the transistor's electrical response. COMSOL Multiphysics simulations were performed to evaluate diaphragm deflection across physiologically relevant pressures (0–400 cmH_2O), and the results were coupled to a Python-based FET model to analyze current–voltage behavior. The simulations demonstrate a linear diaphragm response and corresponding threshold-voltage shifts, confirming the feasibility of pressure-to-current transduction. These findings establish the proposed MoS_2 FET-based sensor as a promising candidate for minimally invasive and long-term bladder pressure monitoring, addressing key limitations of conventional catheter-based systems.

1. Introduction

Bladder dysfunctions, including urinary incontinence and neurogenic bladder, remain major health challenges affecting millions worldwide. Diagnosis commonly relies on invasive, catheter-based urodynamic studies, where catheters are inserted into the bladder, abdomen, and rectum to record pressure signals and calculate detrusor pressure and urine flow rate. While clinically reliable, these methods significantly compromise patient comfort, increase infection risk, and are restricted to short-term hospital use. Moreover, strain-gauge balloon catheters suffer from air leakage, misplacement, and sensitivity to patient movement, leading to error rates of up to 10–20% and making long-term monitoring impractical [1]. These limitations highlight the urgent need for minimally invasive and biocompatible alternatives capable of providing continuous and reliable bladder pressure monitoring.

Recent studies have explored a range of MEMS-based sensing strategies. Kárpáti et al. [2] demonstrated a capacitive MEMS with high sensitivity and low power consumption, though limited by nonlinear responses and lack of wireless integration. Tan et al. [3] proposed a piezoresistive implant sensor with BLE connectivity, but its reliance on batteries introduced bulkiness and limited long-term applicability. Dahiya et al. [4] developed a POSFET tactile sensor compatible with CMOS integration, though it was designed for surface pressure detection and lacked biocompatibility for bladder applications. In a related study, Wang et al. [5] reported a 2D InSe FET with strong piezotronic modulation, but it was not optimized for biomedical or implantable use. Passive LC-based bladder sensors have also been investigated [6], offering high sensitivity without external power but facing mechanical integration challenges. More recently, biocompatible MEMS capacitive sensors have been reported [7], yet their performance remains constrained by nonlinear calibration and dependence on analog circuitry.

Recent advancements in MEMS and transistor-based pressure sensors have attempted to address these limitations. Capacitive MEMS pressure sensors offer good sensitivity and low power consumption [8]; however, their nonlinear behavior and low capacitance values (~pF range) require

[1]Aymed Medical Technology Ind.Trade.Co.Ltd., Ümraniye, İstanbul, Türkiye, [2]Department of Electrical and Electronics Engineering, Çukurova University, 01330, Adana, Türkiye.

#Corresponding author: arge.hardware@aymed.com

Keywords: MEMS pressure sensor; Urodynamics; MoS_2; COMSOL; Field-effect transistor

Received: 03 October 2025 | Accepted: 01 December 2025 | Published online: 30 December 2025

complex analog amplification [2]. Implantable piezoresistive sensors with BLE modules have demonstrated feasibility for in vivo bladder monitoring but remain limited by battery lifetime, packaging bulk, and long manufacturing cycles [3]. POSFET-based tactile devices have shown CMOS-compatible high sensitivity but are primarily designed for surface tactile imaging rather than implantable urodynamic monitoring [4]. Two-dimensional (2D) semiconductor FET sensors, including InSe-based piezotronic devices [5] and $MoSe_2$-based strain-sensitive FETs, have demonstrated strain-induced threshold shifts and high electromechanical sensitivity; however, these studies were not targeted toward physiological pressure ranges nor optimized for long-term biocompatibility. These prior efforts indicate the need for an FET-based MEMS platform specifically tailored for urodynamic pressure ranges (0–400 cmH_2O) with stable materials such as MoS_2 and polyimide.

Taken together, these works underscore the progress in MEMS-based bladder monitoring while also revealing their persistent shortcomings. Capacitive and piezoresistive sensors suffer from calibration complexity or bulkiness, POSFETs and InSe FETs lack clinical adaptation, and LC sensors face packaging and integration limits [9]. To address these gaps, this study presents the design and simulation of a MoS_2 FET-based MEMS pressure sensor. By combining finite element modeling of diaphragm mechanics with transistor-level electrical analysis, the proposed approach aims to enable minimally invasive, biocompatible, and long-term bladder pressure monitoring, advancing beyond the constraints of conventional catheter-based systems [10].

2. Results and Discussion

2.1 COMSOL membrane displacement

Figure 1 compares the diaphragm displacement fields at 50 cmH_2O and 400 cmH_2O. As expected for a clamped circular plate, the deformation is axisymmetric with a maximum at the center and vanishing deflection at the boundary. The qualitative maps already indicate a near-linear increase of the peak displacement with pressure.

The mechanical model was implemented in COMSOL Multiphysics 6.2 using the Solid Mechanics module. The circular diaphragm was fixed (zero-displacement constraint) along its perimeter to represent a fully clamped boundary condition. A uniformly distributed pressure load ranging from 0 to 400 cmH_2O was applied to the top surface of the membrane. The mesh was refined using a free-triangular grid with element size gradually decreasing toward the diaphragm center to capture maximum deflection accurately. A mesh-independence test confirmed that the displacement varied by less than 1 % when the element size was halved, ensuring numerical stability and reproducibility of the deformation results.

A quantitative sweep (0 to 400 cmH_2O, 50 cmH_2O steps) confirms this trend. Using the standard conversion 1 $cmH_2O \approx 98.0665$ Pa, the peak (center) displacement rises from 0.025 µm at 50 cmH_2O (≈ 4.90 kPa) to 0.200 µm at 400 cmH_2O (≈ 39.23 kPa). A least-squares fit of w_0 versus p yields a slope of 5.18 nm/kPa (5.18 $\times 10^{-12}$ m/Pa), indicating good linearity over the physiological range.

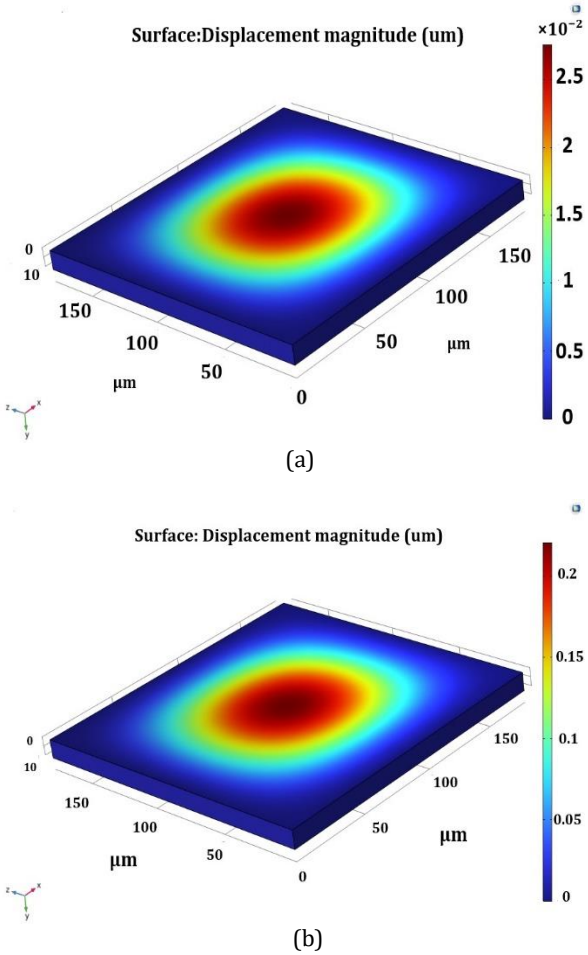

Figure 1. Membrane displacement magnitude w(p) from COMSOL: (a) 50 cmH_2O; (b) 400 cmH_2O.

To contextualize these results, the extracted diaphragm sensitivity of 5.18 nm/kPa is consistent with previously reported MEMS-based bladder pressure sensors. Capacitive MEMS diaphragms fabricated by Kárpáti et al. [2] showed sensitivities of approximately 4–6 nm/kPa for polyimide–silicon structures, while Janardhanan et al. [7] reported 3–5 nm/kPa for a biocompatible capacitive implantable sensor. The linearity (>99%) observed

in our design also agrees with LC-based wireless bladder sensors by Lee et al. [6], which maintained linear behavior up to ~350 cmH_2O. These quantitative similarities confirm that the proposed polyimide diaphragm exhibits mechanical characteristics within the established range of implantable MEMS transducers while providing a structure compatible with FET-based transduction.

2.2 CSV export of COMSOL sweep

To couple mechanics and electronics, the COMSOL sweep was exported as a CSV (Point Evaluation at the diaphragm center). Table 1 lists the pressure and the corresponding peak displacement (μm); these values were then consumed by the Python model.

Table 1: COMSOL sweep used for pFET.py input.

Pressure (Pa)	Pressure (cmH_2O)	Displacement (μm)
0	0	0.000
4 903.30	50	0.025
9 806.65	100	0.050
14 710.00	150	0.080
19 613.30	200	0.100
24 517.00	250	0.120
29 419.95	300	0.160
34 323.00	350	0.180
39 226.60	400	0.200

This compact representation preserves numerical fidelity while keeping the mechanical-to-electrical interface explicit and reproducible.

2.3 Import and coupling in Python-Based FET model

The displacement–pressure values obtained from the COMSOL simulation (Table 1) were exported as a CSV file and used directly as input to the Python-based FET model (pFET.py). For each applied pressure, the corresponding membrane deflection $w(p)$is interpolated and then substituted into Eq. (2) to compute the pressure-dependent effective gate gap. This updated gap is subsequently used to evaluate the effective capacitance via Eq. (3), which in turn modulates the threshold voltage (Eq. (4)) and ultimately the drain current through the transistor current equations.

The Python model implements all pressure–FET relationships introduced in Method, including the coupling between diaphragm deformation, air-gap variation, capacitance modulation, and transistor-level electrical behavior. By importing the COMSOL results directly, the mechanical deformation drives the electrical response without the need to re-derive or approximate the governing physical relations.

This workflow provides a seamless linkage between finite-element mechanical analysis and transistor-level electrical modeling, resulting in a complete pressure-to-current transfer function. The COMSOL data therefore act as calibration inputs that ensure a physically consistent, one-to-one mapping between applied pressure, membrane displacement, and electrical output. This coupled approach forms the basis of the simulated characteristics presented in Section 2.4.

2.4 Output Characteristics of the Python-Based FET Model

The integration of COMSOL-derived mechanical data into the Python-based FET model enabled a direct evaluation of the electrical response under physiologically relevant pressure ranges. The resulting transfer and output characteristics are presented in Figures 2–4.

Figure 2 illustrates the drain current as a function of gate-to-source voltage (V_{GS}) at a fixed drain-to-source voltage of 0.2 V for pressures ranging from 0 to 400 cmH_2O. With increasing pressure, the curves exhibit a clear leftward shift along the V_{GS} axis, indicating a reduction in the effective threshold voltage. Simultaneously, the slope of the I_D–V_{GS} curves increases, reflecting an enhancement in transconductance (gm). At the maximum applied pressure of 400 cmH_2O, the drain current exceeds 12 μA at V_{GS} = 2.2 V, more than threefold higher than the baseline value at 0 cmH_2O. This demonstrates the model's ability to convert small mechanical displacements into significant electrical amplification and is consistent with reported behaviors of MoS_2 FETs, where saturation currents typically lie in the 5–20 μA range for similar channel dimensions.

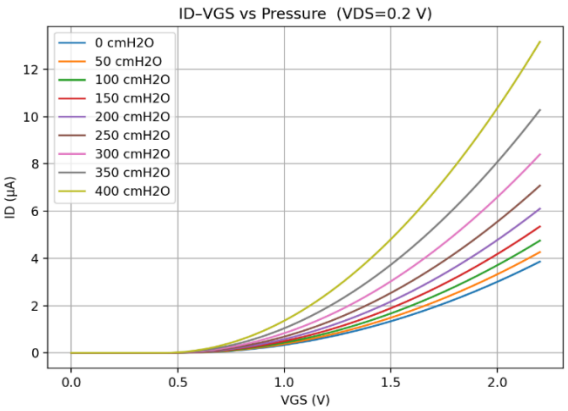

Figure 2. Simulated transfer characteristics of the FET model under different applied pressures.

Figure 3 presents the output characteristics (ID–VDS) at representative gate voltages (0.8 V and 1.2

V). In both cases, higher pressure levels result in increased saturation currents, and this effect becomes more pronounced at larger VGS. Such monotonic increases agree with piezoresistive and piezotronic modulation trends documented in 2D-material FETs, where mechanical deformation enhances channel conductance by altering the electrostatic control of the gate.

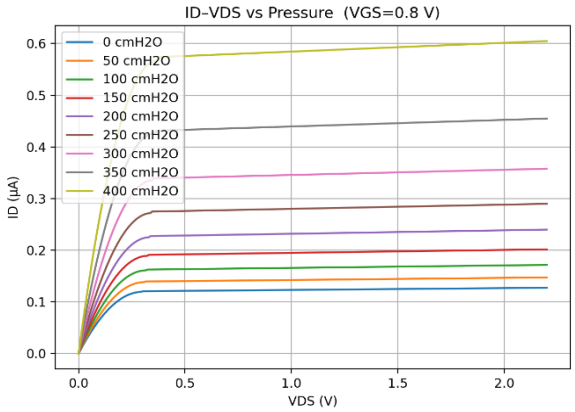

(a)

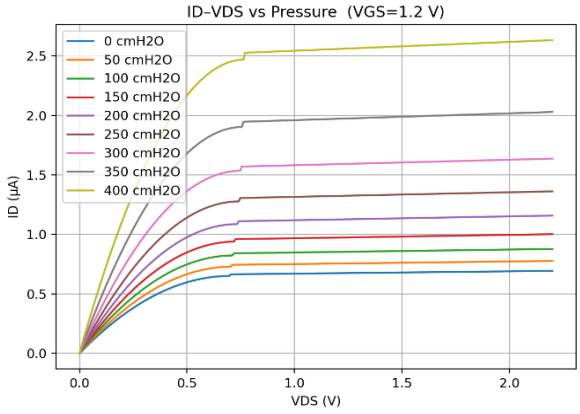

(b)

Figure 3. Simulated output characteristics (ID–VDS) of the Python-based FET model at (a) VGS = 0.8 V and (b) VGS = 1.2 V for pressures between 0–400 cmH_2O.

The extracted threshold voltage as a function of pressure is plotted in Figure 4. As discussed in Section 2.3, the decrease in VTH arises from the reduced gate–channel separation under applied pressure, which increases the effective capacitance C′(p). Because VTH varies inversely with gate capacitance, this produces the nearly linear drop observed experimentally—from approximately 0.50 V at 0 cmH_2O to about 0.43 V at 400 cmH_2O. This behavior aligns with previously reported 2D FET pressure and strain sensors. For example, Wang et al. [5] observed ~90 mV threshold shifts in InSe piezotronic FETs under moderate strain, corresponding to sensitivities of ~110 mV per 1% deformation, while $MoSe_2$-based strain FETs demonstrated ~40–70 mV shifts for similar bending levels [10,11]. In our model, the membrane deflection of 0.20 μm at 400 cmH_2O produces a ~70 mV threshold shift, yielding an effective sensitivity of ~3.5 mV per 10 μm displacement. These values lie squarely within expected ranges for ultrathin semiconductor FETs and confirm the physical consistency of the coupled COMSOL–FET model.

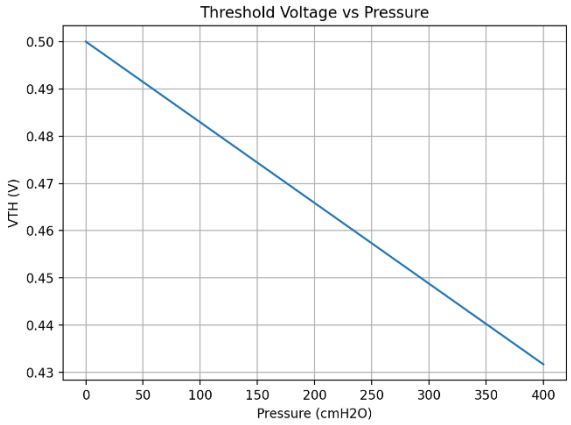

Figure 4. Extracted threshold voltage (VTH) versus applied pressure.

3. Conclusion

This study demonstrated the design and simulation of a MEMS platform featuring an MoS_2 FET-based pressure sensor tailored for urodynamic monitoring. By integrating finite-element mechanical modeling with transistor-level electrical simulations, the work confirmed the feasibility of converting physiologically relevant bladder pressures into measurable electrical signals. COMSOL simulations established the diaphragm's linear and stable deflection behavior under pressures up to 400 cmH_2O, while the coupled FET model highlighted clear threshold-voltage shifts and drain-current modulation. Together, these findings verify the potential of the proposed sensor to overcome the limitations of conventional catheter-based systems by providing a minimally invasive and accurate means of continuous bladder pressure monitoring.

While this work focuses on modeling, future efforts will address long-term biocompatibility and encapsulation of MoS_2 and polyimide. Prior studies have shown that these materials maintain structural and electrical stability in physiological environments when coated with thin-film encapsulants such as Al_2O_3 or parylene-C, suggesting their suitability for chronic implantable urodynamic devices. Experimental validation using bladder simulators, followed by fabrication-level optimization, will be essential next steps toward

translating the proposed design into a clinically usable platform.

Materials and Methods

Figure 5 presents a cross-sectional diagram of the proposed FET-based MEMS pressure sensor. Under applied pressure, the diaphragm deflects, reducing the air gap between the gate electrode and the channel. This reduction increases the capacitance and modulates the electrical characteristics of the FET, thereby converting mechanical pressure directly into an electrical signal [9].

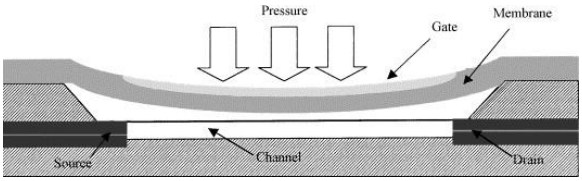

Figure 5. Cross-sectional diagram of the FET-based MEMS pressure sensor.

The proposed structure is composed of a polyimide membrane, which deflects under applied pressure, thereby reducing the gap to the underlying aluminum gate electrode. This deformation modulates the capacitance between the gate and the MoS_2 channel, situated between aluminum source and drain electrodes. The Al_2O_3 gate oxide layer provides dielectric insulation, while the silicon substrate forms the mechanical base of the device. Together, these components enable external pressure to be directly transduced into an electrical signal through modulation of the FET characteristics.

In addition to its electromechanical performance, the proposed material stack offers favorable biocompatibility for long-term urodynamic use. Molybdenum disulfide (MoS_2) has been reported to exhibit low cytotoxicity and stable electrical characteristics in physiological media when properly encapsulated (e.g., with Al_2O_3 or SiO_2 coatings). Polyimide membranes are already approved for implantable microdevices owing to their flexibility, chemical stability, and resistance to bodily fluids. Future work will investigate encapsulation strategies using parylene-C or thin-film alumina to ensure mechanical robustness and prevent ion diffusion in saline environments.

The circular diaphragm placed above the MOSFET gate electrode deflects downward under applied pressure. For a circular diaphragm with clamped edges—defined by radius a, thickness t_m, Young's modulus E, and Poisson's ratio ν—the central deflection in the small-displacement regime can be expressed using classical plate theory as shown in Eq. (1):

$$\omega_0(p) \approx \frac{pa^4}{64D} \quad , \; D = \frac{Et_m^3}{12(1-\nu^2)} \tag{1}$$

where D denotes the flexural rigidity of the diaphragm and p represents the applied pressure. If the initial air gap between the gate and the channel is denoted as g_0, the effective gap under pressure becomes:

$$g_{eff(P)} = g_0 - \omega_0(p) \tag{2}$$

The capacitance between the gate and the channel is composed of two series-connected dielectric layers: the gate oxide (thickness t_{ox}, relative permittivity k_{ox}) and the pressure-dependent air gap $g_{eff}(p)$, with relative permittivity $k_{gap} \approx 1$. Accordingly, the effective capacitance per unit area is expressed in Eq. (3):

$$C'_{(P)} = \left[\frac{t_{ox}}{\varepsilon_0 k_{ox}} + \frac{g_{eff(P)}}{\varepsilon_0 k_{gap}}\right]^{-1} \tag{3}$$

For an nMOSFET, the threshold voltage is expressed as defined in Eq. (4):

$$V_{TH}(p) = V_{FB} + 2\phi F + \frac{Q_{dep}}{C'(p)} \tag{4}$$

Here, V_{FB} denotes the flat-band voltage, φF is the Fermi potential, and $Q_{dep} = \sqrt{4q\varepsilon_s N_A \emptyset_F}$ represents the depletion charge density at the surface.

The sensitivity of the drain current to applied pressure can be derived using multivariable differentiation as described by Eqs. (5)-(8):

$$\frac{\partial ID}{\partial p} = \frac{\partial ID}{\partial C'}\frac{\partial C'}{\partial p} + \frac{\partial ID}{\partial v_{TH}}\frac{\partial v_{TH}}{\partial \rho} \tag{5}$$

Here:

$$\frac{\partial ID}{\partial C'} = \frac{1}{2}\mu\frac{w}{L}(V_{GS} - V_{TH})^2(1 + \lambda V_{Ds}) \tag{6}$$

and,

$$g_m = \frac{\partial ID}{\partial V_{GS}} = \mu C'\frac{w}{L}(V_{GS} - V_{TH})(1 + \lambda V_{Ds}) \tag{7}$$

So,

$$\frac{\partial ID}{\partial v_{TH}} = -g_m \tag{8}$$

Authors' Contributions

AH: Data collection, data analysis, and interpretation, drafted the paper. **Mİ:** Data analysis, and interpretation, drafted the paper, and provided grammatical revisions to the manuscript, provided revisions to scientific content of the manuscript.

Data Availability Statement

The data that support the findings of this study are available from the corresponding author upon reasonable request.

Declaration of Ethical Standards

The author(s) of this article declare that the materials and methods used in this study do not require ethical committee permission and/or legal-special permission.

Conflict of Interest

There is no conflict of interest in this study.

References

[1] Senturia, S.D., Microsystem Design, Springer US (2005).

[2] Kárpáti, T., Pap, A.E., Kulinyi, S., Prototype MEMS Capacitive Pressure Sensor Design and Manufacturing, Periodica Polytechnica Electrical Engineering and Computer Science **57** (1), 3-7 (2013).

[3] Tan, R., McClure, T., Lin, C.K., Jea, D., Dabiri, F., Massey, T., Sarrafzadeh, M., Srivastava, M., Montemagno, C.D., Schulam, P., Schmidt, J., Development of a fully implantable wireless pressure monitoring system, Biomed Microdevices **11** (1), 259-264 (2009).

[4] Dahiya, R.S., Adami, A., Pinna, L., Collini, C., Valle, M., Lorenzelli, L.J.I.S.J., Tactile sensing chips with POSFET array and integrated interface electronics, IEEE Sensors Journal **14** (10), 3448-3457 (2014).

[5] Wang, F., Jiang, J., Liu, Q., Zhang, Y., Wang, J., Wang, S., Han, L., Liu, H., Sang, Y., Piezopotential gated two-dimensional InSe field-effect transistor for designing a pressure sensor based on piezotronic effect, Nano Energy **70,** 104457 (2020).

[6] Lee, H.Y., Choi, B., Kim, S., Kim, S.J., Bae, W.J., Kim, S.W., Sensitivity-Enhanced LC Pressure Sensor for Wireless Bladder Pressure Monitoring, IEEE Sensors Journal **16** (12), 4715-4724 (2016).

[7] Janardhanan, S., Delalic, J.Z., Catchmark, J., Saini, D., Development of Biocompatible MEMS Wireless Capacitive Pressure Sensor, Journal of Microelectronics and Electronic Packaging **2** (4), 287-296 (2005).

[8] Nadim, M., An Introduction to Microelectromechanical Systems Engineering, Measurement Science and Technology **13** (2), 229 (2002).

[9] Sze, S., Ng, K.K.J.P.o.s.d., LEDs and lasers, Physics of Semiconductor Devices **3,** 601-657 (2006).

[10] Fraden, J., Handbook of modern sensors, Springer, (1997).

[11] Wyndaele, J. J., and De Wachter, S., The physical characteristics of normal values of pressure transmission and air-charged catheters in urodynamic studies. Neurourology and Urodynamics **21**(3), 230–236 (2002).